



An estimation-based approach for range image segmentation: on the reliability of primitive extraction

Guoyu Wang^{a,*}, Zweitze Houkes^b, Guangrong Ji^a, Bing Zheng^a, Xin Li^a

^aDepartment of Electrical Engineering, Ocean University of Qingdao, 266003, Qingdao, People's Republic of China

^bDepartment of Electrical Engineering, University of Twente, 7500 AE Enschede, The Netherlands

Received 3 May 2001; accepted 17 December 2001

Abstract

This paper presents a new algorithm for estimation-based range image segmentation. Aiming at surface-primitive extraction from range data, we focus on the reliability of the primitive representation in the process of region estimation. We introduce an optimal description of surface primitives, by which the uncertainty of a region estimate is explicitly represented with a covariance matrix. Then the reliability of an estimate is interpreted in terms of “measure of uncertainty”. The segmentation approach follows the region-growing scheme, in which the regions are estimated in an iterative way. With the probabilistic model proposed in this paper, surface homogeneity is defined and tested by an optimal criterion. A notable feature of the algorithm is that the order of merging is organized to lead the growth towards the most reliable representation of the merged region. Concerned with man-made objects in the scene, we restrict the class of surface primitives to be quadric or planar. The proposed algorithm has been applied to real data and synthetic data and demonstrated with experimental results. © 2002 Pattern Recognition Society. Published by Elsevier Science Ltd. All rights reserved.

Keywords: Segmentation; Primitive extraction; Uncertainty; Optimal description; Region growing; Quadrics

1. Introduction

Image segmentation can be defined as a process of partitioning a given image into a set of meaningful regions. A meaningful region represents a region in which all pixels possess similar properties. As an outcome of the segmentation, symbolic descriptions are usually applied to model the partitioned regions in high-level modules of a vision system.

Essential in segmentation is the definition of “homogeneity” of partitioned regions. It is often impossible to define the homogeneous property purely from a strict mathematical context, because the expected result of segmentation is

controlled by the whole recognition or measurement strategy of a vision task. For 2D gray-level images, the homogeneity criterion can be based on segments of “visually pleasing regions” [1], i.e., segments of the image are in accordance with our perceptual experience about the pattern of illumination. But such intuitive visual judgement is meaningless for 3D data. In fact, in segmentation of range images, the partitioning principles not only depend on the nature of the input image, but also on the kind of symbolic representations of the objects, because any segmentation task must be put in perspective with the final objective of a vision system. Especially in a model-based recognition system, the low-level segmentation routine is highly interrelated to the strategy of representation of the objects.

The methods of range image segmentation can be briefly classified into two approaches: region-based (e.g. Refs. [1–7]) and edge-based (e.g. Refs. [8–12]). In region-based methods, pixels having similar properties are grouped together and finally the images are partitioned into a set of

* Corresponding author. Tel.: +86-532-2032966; fax: +86-532-2032799.

E-mail address: gywang@mail.ouqd.edu.cn (G. Wang).

¹ This work was done in the Measurement & Instrumentation Laboratory, University of Twente, The Netherlands.

homogeneous regions. In surface-based object representations, such a homogeneous region is modeled with a surface primitive one. From this point of view, the task of range image segmentation is in fact a process of primitive extraction and the homogeneity is defined on the parameterized model of the surface primitive. Thus, a homogeneous region is thought to “fit well” the parametric description, whereas two regions are thought to be homogeneous if they can be expressed as two observations of the same surface primitive.

Critical in a region-based approach is the clustering of data subsets. Basically, a homogeneity test determines the process of clustering. However, errors in the estimates of region parameters are inevitable because of the noise in the range data. Therefore, the reliability of the homogeneity test by estimation-based algorithms could suffer from the lack of explicit representation of uncertainties of region estimates. In Ref. [13], a Bayesian segmentation methodology is proposed with parameterized models. In that approach, instead of direct parameter estimation, a so-called “probability of homogeneity” is derived from the a posteriori probability conditioned by two joint observations in the spatial domain. Thus, the uncertainties in the region’s parameters are considered in the homogeneity test in an implicit way. Although that methodology provides an optimal test of homogeneity between regions using parameterized models, it is still unknown as to how a homogeneous region “fits” the used model, because no parameters are estimated in that approach.

In this paper, we present a new algorithm of region-based approach. It is based on the optimal description of surface primitives, with which the uncertainties in the estimates of region parameters are explicitly represented with a probabilistic model. In the optimal description of surface primitive, the region parameters are estimated through a fitting procedure. The uncertainties of the estimates are represented with the covariance matrix of the region parameters, which is formulated simultaneously in region estimation. Consequently, we propose a probabilistic model with normal pdf to characterize the statistical properties of the estimates of the primitives. Then the criterion for homogeneity test in region clustering is established on Bayesian principle. Therefore, an estimation-based optimal clustering algorithm can be implemented, with equal optimality of the approach of Ref. [13]. However, the degree of fitting of a homogeneous region to a modeled primitive is represented as well. It means that the reliability of primitive extraction can be evaluated.

Often a problem that occurred in the existing region growing approach is that the segmentation results rely on the order of merging the subset of data in the growing process. To control the reliability of primitive extraction in an estimation-based segmentation routine, we define a metric of “measure of uncertainties” to describe the reliability of a region estimate. Therefore, the order of merging is organized to let the segmentation process converge to the “most reliable” representations of surface primitive.

Commonly used parameterized models in segmentations are piecewise polynomials [2,11,12,14–16]. Low degree polynomials, i.e. degree 1 or 2, have been popular in modeling smooth curved surface primitives, especially in industrial applications [3,17]. In this paper, we focus on the quadric and planar representations of surface primitives. One should note that such simple primitives are powerful in modeling even more complicated objects, using the *relational structure* representation (RS).

2. Optimal description of region parameters

To yield the result of segmentation of a range image described as a list of surface primitives, our approach is driven by surface-based representations of the range data. In this section, we briefly introduce the optimization in region-based parameter estimation, with which the uncertainties of estimated parameters are explicitly formulated in region estimation.

2.1. Modeling the uncertainties of surface parameters with a covariance matrix

In reality, the performance of uncertainties in parameter estimation could be very complicated and it is impossible to perfectly fit an analytical mathematical model. Here, we use the covariance matrix of an estimate to characterize the major statistical features of the uncertainties. To formulate the covariance matrix, we utilize a perturbation analysis of the errors of the estimated parameters in surface fitting.

2.1.1. Covariance matrix of a quadric representation

The region parameters are estimated through fitting the 3D data points to a quadric or a planar representation. For the estimation of quadric primitives, we applied the improved *renormalization* method (the readers are referred to Refs. [7,18,19] for details of the parameter estimation). A remarkable feature of this method is its “bias-corrected” optimization in parameter estimation, while the variance of noise is estimated simultaneously in the fitting process. The unbiased property of the estimate also suggests linear approximation in the error representation of the parameters with respect to the noise in data points.

A quadric primitive can be expressed in an implicit form

$$f(x, y, z) = a_{11}x^2 + a_{22}y^2 + a_{33}z^2 + a_{12}xy + a_{13}xz + a_{23}yz + v_1x + v_2y + v_3z + k = 0. \quad (1)$$

Keeping the scale constraint $k = 1$, we define a parameter $\theta = [a_{11}, a_{22}, a_{33}, a_{12}, a_{13}, a_{23}, v_1, v_2, v_3]^T$ vector to represent the surface primitive.

Θ denotes the cost function of surface-fitting and given a set of data points $\{\mathbf{x}_i\}_{i=1}^n$, the estimate $\hat{\theta}$ is obtained by solving the minimization problem $(\partial\Theta/\partial\theta) = 0$. The cost function Θ is established on the gradient-weighted least-squares

criterion, defined as $\Theta = \sum_{i=1}^n d_i^2$, where $d_i \forall i = 1, \dots, n$ is the geometric distance between the point \mathbf{x}_i and the surface. We can take the Taylor expansion of d_i^2 up to a second-order approximation of $\Delta\theta$ and $\Delta\mathbf{x}_i \forall i = 1, \dots, n$, where $\Delta\mathbf{x}_i$ is the noise perturbation and $\Delta\theta$ is the error in the estimated parameter $\hat{\theta}$. Assuming that $\Delta\mathbf{x}_i \forall i$ is an independent, identical distributed (iid) Gaussian noise, we have the expression of the covariance matrix of $\hat{\theta}$ as [7]

$$\Psi = \sigma^2 \left(\sum_{i=1}^n w_i \mathbf{m}_i \mathbf{m}_i^T \right)^{-1} \quad (2)$$

where $\mathbf{m}_i = [x_i^2, y_i^2, z_i^2, x_i y_i, x_i z_i, y_i z_i, x_i, y_i, z_i]^T$; $w_i = 1/\|\nabla f(\mathbf{x}_i)\|^2$.

2.1.2. Covariance matrix for a planar representation

Normally, a planar surface can be represented by the implicit form

$$\mathbf{n}^T \mathbf{x} + \mathbf{b} = 0, \quad (3)$$

where $\mathbf{n} = [n_x, n_y, n_z]^T$ is the unit normal vector of the plane. By defining the surface parameter vector

$$\theta_{nb} = [\theta_n^T, b/n_z]^T, \quad (4)$$

where

$$\theta_n = [n_x/n_z, n_y/n_z]^T \quad (5)$$

we can derive the covariance matrix of θ_{nb} . Analogous to the way of modeling uncertainties in the quadric representation, the covariance matrix of θ_{nb} is formulated with the expression [7]

$$\Psi_{nb} = \sigma^2 \mathbf{M}_p^{-1}. \quad (6)$$

For the purpose of segmentation with surface primitives, what we are concerned with is only the normal vector θ_n , which is associated to the discontinuity of planar regions. Consequently, the covariance matrix for the parameter vector θ_n , denoted as Ψ_n , is obtained as the top-left 2×2 matrix of Ψ_{nb} .

There has been research work concerning the formulation of uncertainties in object descriptions. Waite and Ferrie [20] discussed the non-uniqueness problem in volumetric representations. They characterized the ambiguity of parameter estimates in terms of the “ellipsoid of confidence”, quantifying the level of acceptability of a model and the information that can be used to plan a new direction of view that minimizes the ambiguity of subsequent interpretation. But as was argued by the authors, the representation was limited to partially communicating non-uniqueness at a single minimum in parameter space. The work of Subrahmonias et al. [16] dealt with the object in higher order polynomial representations. They used the asymptotic form of estimates to describe the posterior distribution of the parameters in polynomial fitting, and a criterion of minimum-error-probability for recognition was proposed. However, the reality of their probabilistic model, especially the derivation of covariance

information, relies on the assumption that a large number of data are involved in fitting. Moreover, the knowledge of noise perturbation in data acquisition was not adequate for the description of the uncertainties in parameter estimation.

Unlike the work of Subrahmonias et al. [16] and Whaite and Ferrie [20], we formulate the covariance matrix of the estimated parameters from the linear dependency of the perturbation $\Delta\theta$ on the noise $\{\Delta\mathbf{x}_i\}$. This linear assumption is applicable in the case of a moderate level of noise in data acquisition. However, since the estimate of $\Delta\theta$ is statistically unbiased, the linear dependency is expected to be tolerant to even a significant level of noise perturbation. It should be noticed that the derivation of the covariance matrix in Eq. (2) does not rely on the asymptotic assumption, so it is more applicable to region-based estimation than the way it is used in Ref. [16].

2.2. Definition of homogeneity based on the optimal description of surface primitive

Given the “unbiased” estimate of a region parameter $\hat{\theta}$ and its covariance matrix Ψ , we proposed an analytical probabilistic representation to model the estimate of $\hat{\theta}$. This representation is suggested considering a few aspects: (1) the covariance matrix Ψ is derived from the approximation of the linear dependency in Eq. (1). Since the noise $\{\Delta\mathbf{x}_i\}$ is assumed as Gaussian noise, the perturbation $\Delta\theta$ is consequently approximately normally distributed; (2) the gradient weighted LSE can be interpreted [16] in terms of *maximum likelihood estimation* (MLE), whose asymptotic distribution is normal. Briefly, the first- and second-order statistics reveal the major statistical behavior of an estimate. Thus, the normal pdf is a tractable model since it describes all the statistics of the estimate by the expectation and the covariance.

Denoting by θ the “true” parameters describing the surface primitive and with $\hat{\theta}$ an estimate obtained from the measurements, the normal pdf of $\hat{\theta}$ is expressed by

$$f(\hat{\theta}|\theta) = C \exp\{-\frac{1}{2}(\hat{\theta} - \theta)^T \Psi^{-1}(\hat{\theta} - \theta)\}, \quad (7)$$

where C is the normalized constant.

In reality, the true θ is unknown. To test the homogeneity of two regions, what we are concerned with is in fact a probabilistic representation that two estimates come from the same primitive, irrespective of the true parameters of that primitive.

Suppose that $\hat{\theta}_1$ and $\hat{\theta}_2$ are two estimates from measurements, the *likelihood* of the homogeneity condition that $\hat{\theta}_1$ and $\hat{\theta}_2$ are two observations of the same surface primitive is expressed by the joint pdf of $\hat{\theta}_1$ and $\hat{\theta}_2$ as

$$\begin{aligned} f(\hat{\theta}_1, \hat{\theta}_2|H) &= \int f(\hat{\theta}_1, \hat{\theta}_2|\theta) d\theta \\ &= \int f(\hat{\theta}_1|\theta) f(\hat{\theta}_2|\theta) d\theta. \end{aligned} \quad (8)$$

Substituting Eq. (7) into Eq. (8) and assuming that the covariance matrices both for $\hat{\theta}_1$ and $\hat{\theta}_2$ are unchanged in the integration, the integration of Eq. (8) yields the following expression:

$$f(\hat{\theta}_1, \hat{\theta}_2 | H) = C \exp\{-\frac{1}{2}(\hat{\theta}_1 - \hat{\theta}_2)^T \Psi_{1,2}^{-1}(\hat{\theta}_1 - \hat{\theta}_2)\}, \quad (9)$$

where C is again the normalized constant and

$$\Psi_{1,2} = \Psi_1 + \Psi_2. \quad (10)$$

In Eq. (10), Ψ_1 and Ψ_2 are the covariance matrices for $\hat{\theta}_1$ and $\hat{\theta}_2$ that are independently obtained from the measurements.

According to (9), the homogeneity test can be implemented in the probability space as a *hypotheses test* problem. The hypotheses are stated as

$$\begin{aligned} H_0: & E\{\hat{\theta}_1\} = E\{\hat{\theta}_2\} \quad (\text{homogeneous}); \\ H_1: & E\{\hat{\theta}_1\} \neq E\{\hat{\theta}_2\} \quad (\text{inhomogeneous}). \end{aligned}$$

We define an “optimal distance” as

$$d_{1,2}^2 = \frac{1}{2}(\hat{\theta}_1 - \hat{\theta}_2)^T \Psi_{1,2}^{-1}(\hat{\theta}_1 - \hat{\theta}_2), \quad (11)$$

used to test the hypothesis. Given a selected threshold T_d , if $d_{1,2}^2 \geq T_d$, then H_0 is rejected and H_1 is accepted, meaning that $\hat{\theta}_1$ and $\hat{\theta}_2$ are inhomogeneous. Otherwise, they are thought to be homogeneous. The threshold T_d is associated with the so-called *significance level*, denoted by α , which can be expressed as $T_d = T(\alpha)$. Theoretically, the value of α can be chosen according to the design of the probability of the type-1 error. In practice, however, because the covariance computation was derived approximately, the threshold T_d still needs to be determined empirically.

2.3. Definition of the reliability of a region estimate

In region-based segmentation, two regions are merged if they are tested as homogeneous. After the merging, however, we still need to know in what degree the current region fits a primitive representation. In other words, for primitive extraction, a region-based segmentation process must account for the *reliability* of the estimate of a region. Such a reliability of an estimate can also be quantified in the sense of homogeneity test with respect to a single region.

Since the covariance matrix Ψ of an estimate represents the uncertainty in estimation, we define a metric of “measure of uncertainty”, denoted by M_{unct} , to characterize the reliability of a region estimate:

$$M_{unct} \equiv \|\Psi\|_2 \quad (\text{measure of uncertainty}). \quad (12)$$

Hence, the larger the M_{unct} , the lesser is the reliability of the estimated region and vice versa.

It should be pointed out that the “measure of uncertainty” is defined on the parametric domain, rather than the spatial domain. Naturally, the smaller the noise level, the smaller are the errors in parameter estimation. But in spatial domain, the residue of the cost function only reveals the noise level, and so partially communicates the uncertainties of the

estimate. However, the uncertainty in parametric domain not only relies on the noise variance, but also relies on the *observability* of the formation of the problem. Typical of the case resulting in a large measure of uncertainty is the ill-posed solution of the estimate.

3. The algorithm of the estimation-based segmentation

In this section, we describe the algorithm of segmentation based on the optimal description of surface primitives. A flowchart of the approach is depicted in Fig. 1.

The approach consists of three modules. In order to hold the generic constraints of piecewise smoothness for region estimation, outliers are extracted from the input range data in the first module. Here, the outliers are defined as either error data points or discontinuity points (i.e., edge or boundary points). This is achieved by fitting the data points in a small sampling window to a planar description and testing the goodness of fit. The central point of the window whose planar fitting is recognized as “bad” is marked as an outlier. By moving the sampling window over the whole range image, centered at each pixel each time, we extract the outliers of the input range image. In the second module, the

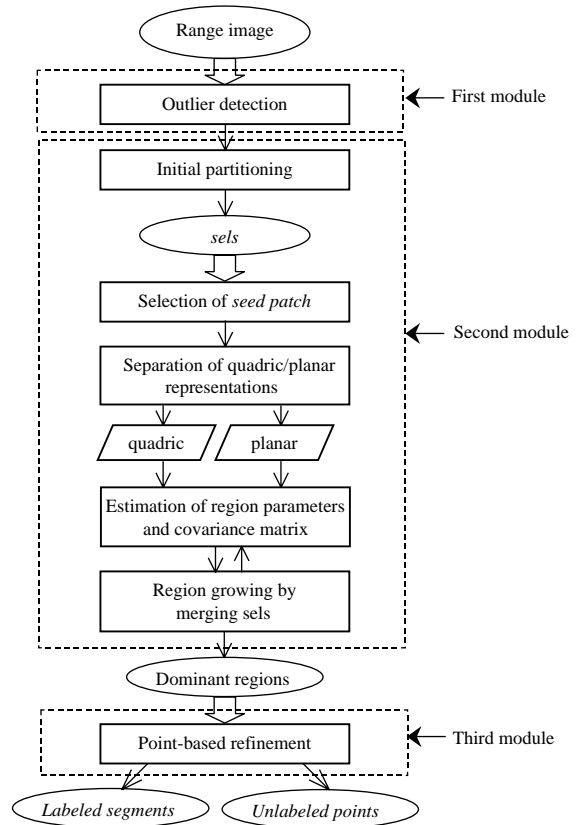


Fig. 1. Flowchart of the segmentation algorithm.

whole image is initially partitioned into small regions with a rectangular grid pattern. Following Ref. [15], these initial grid regions are noted as “surface elements”, or *sels*. These sels then pass through the merging process, according to the criterion of homogeneity test. The merging process starts with a seed of subregions consisting of a few neighboring sels. Such a group of neighboring sels is denoted as a *patch*. When the growth of a patch stops, a new patch is selected and the process repeats until no more seeds can be found. At the end of the second module, the merged sels represent several isolated segments with different labels in the range image. Such a segment is denoted as the *dominant region*. In the last module, a process of point-based refinement is applied, with which the points near the boundary of dominant regions are reclassified according to a measure of the distance between the point and the estimated surface.

In estimation of the seed patch, a planarity test is applied according to the result of the quadric fitting of the seed patch. If the seed turns out to be planar, then it is represented as a planar patch and the region-growing process is carried out using the planar representation. Otherwise, the seed and its updated region are estimated through a quadric representation.

Finally, the outcomes of the segmentation include the labeled regions, either in quadric or planar representations, and the unlabeled points.

3.1. Outlier detection

Given the input range data, a small rectangular window is used as the mask to test the local geometry of each point. The size of the window is pre-defined, according to the sampling resolution of the range data as well as the size of the objects in consideration. As an example, the window size used in our experiments is 5×5 (point²). Obviously, if the window covers the boundary and partially embeds different object surfaces or different objects, or contains any local irregularity of an object, then this region will show a bad fitting to a planar representation and then the centre point of the window will be considered as an outlier.

Treating the points $\{\mathbf{x}_i, i = 1, \dots, m\}$ sampled within the window as 3D random points, we compute the eigenvalues of the matrix

$$\mathbf{Z} = \frac{1}{m-1} \sum_{i=1}^m (\mathbf{x}_i - \bar{\mathbf{x}})(\mathbf{x}_i - \bar{\mathbf{x}})^T, \quad (13)$$

where $\bar{\mathbf{x}} = (1/m) \sum_{i=1}^m \mathbf{x}_i$.

The smallest eigenvalue of \mathbf{Z} , denoted by c_{min} , can be used as a measure of planarity of these points. If c_{min} exceeds a threshold, i.e., if $c_{min} \geq T_{win}$, then this patch is thought to be inhomogeneous and the central point is classified as an outlier. For robust detection, the threshold is set by

$$T_{win} = r_{win} c_{min}, \quad (14)$$

where \tilde{c}_{min} is the median of c_{min} for all the windows in the range data, and r_{win} is a chosen constant.

In parallel, if the difference in depth values between the center point and its nearest neighboring point exceeds a pre-defined threshold, this center point is also thought to be an outlier.

Moving the window over the entire range image, centered at each point, the outliers are extracted using the above two criteria.

Although the outlier detection in the first module is not critical for the proposed region-based segmentation approach, it provides a preliminary description of the “inhomogeneity” of the scene. More importantly, a successful outlier detection reduces the risk of falsely merging two inhomogeneous regions, as well as the computational burden of surface fitting in the region-growing process. The extracted outliers will be re-evaluated in the third module.

3.2. Estimation-based region-growing scheme

After detection of outliers, the range image passes through the estimation-based region-growing stage. Initially, the range image is manually partitioned into a set of regular grid pattern. Then the region-growing process starts with these over-segmented small partitions, i.e., *sels*. Selecting the size of a sel is done manually. On the one hand, it should be sufficiently small so that points from a smooth surface lying within the sel are thought to be homogeneous and planar descriptive. On the other hand, an extremely small size of the sel might cause difficulties in parameter estimation at the beginning of growing because of insufficient shape information in a very small patch. Moreover, the smaller the sels, the more iterations the updating process takes, and more computational time will be required. In practice, the size of the sel can be set about the same as that of the window used in outlier detection.

If the number of outliers in a sel exceeds a threshold, then it is marked as “ambiguous”, meaning that it may cover a part of the object boundary or local irregularities. Others are termed as “ordinary” sels. Only the ordinary sels participate in the region-growing process. For each of these ordinary sels, the local variance of the noise is estimated with the value of c_{min} as computed in an outlier detection.

The seed for region growing is selected as an array of neighboring sels, a subregion noted as *patch*. In our approach, the type of the array is selected in notion of a second-order *neighborhood system*, treating the grid-pattern sels as “pixels”. So the maximum size of a patch is nine sels and we set the minimum size to six. Starting with such a seed patch, the region grows by merging the neighboring ordinary sels of the current region and the region is updated in an iterative way. This process is controlled by the criterion of the homogeneity test, which can be interpreted as the clustering principle of the sels. The clustering principle is based on the *hypothesis test* implemented with the optimal description of surface representations as stated in Section 2.

Denote the current region at the k th iteration as $R^{(k)}$. For a neighboring sel S , the merged region is represented as

$R^{(k+1)} = R^{(k)} \cup S$. Suppose that (θ_k, Ψ_k) are the estimates of parameters for the current region $R^{(k)}$, where θ denotes the surface parameter vector and Ψ denotes the covariance matrix. After merging the sel S , the estimates for $R^{(k+1)}$ are $(\theta_{k+1}, \Psi_{k+1})$. Assuming that $R^{(k)}$ and S belong to the same surface that can be represented with their primitive representation, then the estimates of the surface parameters θ_k and θ_{k+1} are two observations of the same primitive.

According to the description in Section 2, the homogeneity between the estimates before and after merging can be tested by a measure of the “optimal distance” between $R^{(k)}$ and $R^{(k+1)}$. Now the optimal distance is computed as

$$d_{k,k+1}^2 = \frac{1}{2}(\theta_k - \theta_{k+1})^T \Psi_{k,k+1}^{-1}(\theta_k - \theta_{k+1}), \quad (15)$$

with

$$\Psi_{k,k+1} = \Psi_k + \Psi_{k+1}.$$

If $d_{k,k+1}^2 \geq T_d$, then the merging is rejected, meaning $R^{(k)}$ and S are inhomogeneous. Otherwise, they are thought to be homogeneous and the merging of S with $R^{(k)}$ is acceptable.

Once the sel passes the test and is merged, the region $R^{(k+1)}$ is represented with the updated description $(\theta_{k+1}, \Psi_{k+1})$ and the next neighboring sel is tested. If all the neighboring sels of the current region fail to pass the test, the growing process of the selected seed stops. From the remaining ordinary sels, a new seed patch is selected and the growing process as described above is repeated. The whole process is completed when no more seed patches are found. At the end of this module, the input range image is segmented into several fundamental regions, each of which consists of a set of sels, which are noted as the *dominant regions*. The rest of the range image includes “ambiguous” sels and some ordinary sels, whose number of neighbourhood is less than the minimum requirement of a patch.

We would like to address some new features of the estimation-based merging algorithm.

3.2.1. The order of merging

In general, any segmentation implemented with the region-growing principle meets two fundamental questions: (1) When does the growing stop? (2) In which order should the candidate sels be chosen for merging with the patch?

The answer to the first question is in fact the criterion of the homogeneity test for region-based approaches. The second question, however, has not yet been fully treated until now. An intuitive answer to the second question is that the points adjacent to the current region with the “best” output from the homogeneity test, are given highest priority for merging. For example, the sel that generates the smallest value of $d_{k,k+1}^2$ could be taken into $R^{(k+1)}$ first. However, such a priority only comes from the degree of homogeneity of two estimates, but the degree of reliability of the region’s estimate after merging is neglected. In other words, merging the “best homogeneous” points cannot guarantee the yield of the “best reliable” representation of the updated region $R^{(k+1)}$. This is because the uncertainties in parameter esti-

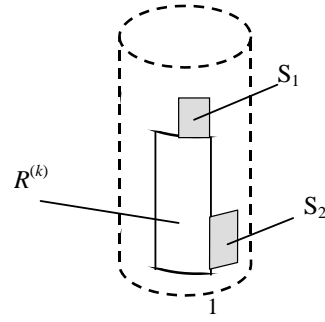


Fig. 2. Selection of the candidate sel for the next merging.

mation not only depend on the noise level of the data points involved in the surface fitting, but also depend on the spatial locations of these points. This can be illustrated with the heuristic example of Fig. 2.

Suppose that the current region $R^{(k)}$ is a rectangular portion of a cylindrical surface whose length extends along the axis of the cylinder, and that both the sels S_1 and S_2 pass the homogeneity test. Intuitively, merging S_1 into $R^{(k)}$ yields the estimate of $R^{(k+1)}$ less reliable than that of merging S_2 into $R^{(k)}$. The merging of S_1 results in an extension of the length of $R^{(k)}$ along the axis, and $R^{(k+1)}$ is still “flat” somehow (assuming its width is narrow compared with the radius of the cylinder), so the parameter estimation of $R^{(k+1)}$ is unstable. On the contrary, merging of S_2 will embed more information of the “curving” of the surface in estimating $R^{(k+1)}$, resulting in a lesser uncertainty in shape description (assuming that the noise level remains the same). Therefore, although S_1 could result in a smaller distance measure between $R^{(k)}$ and $R^{(k+1)}$, the sel S_2 should have a higher priority for merging in view of the *reliability* of surface representation.

In fact, from the expression of the optimal distance of Eq. (11), it can be seen that a large value of the covariance matrix $\Psi_{k,k+1}$ results in a small value of $d_{k,k+1}^2$. However, this does not help to improve the reliability of the representation of the current region $R^{(k+1)}$.

According to the above argument, in the proposed approach, the merging priority in the region-growing process is determined by the “measure of uncertainty” M_{unct} as defined in Eq. (12). Therefore, among all the neighboring sels that pass the homogeneity test, the one that generates the smallest M_{unct} is merged first. In order to reduce the burden of parameter estimation for each candidate sel, in practice, the value of M_{unct} is estimated only by approximation. Instead of recomputing the region parameters after merging each sel, the current estimate θ_k is used for the computation of M_{unct} , just by adding data points of each sel into the current group of points in $R^{(k)}$. Thus, the sel with the smallest M_{unct} has the highest priority of passing through the homogeneity test. If it fails to pass the homogeneity test, then we choose the next in the queue ordered by the value of M_{unct} from the smallest to the largest.

3.2.2. Selection of the seed patch

Although there is more than one candidate of the *patch* to be selected as the seed of growing, an optimal choice is still based on the reliability of representation in surface estimation. Following the same principle as discussed above, the patch with the smallest measure of uncertainty $\|\Psi_{patch}\|_2$ is selected as the seed. Here, Ψ_{patch} is the covariance matrix estimated in fitting data points in the patch to the quadric representation. It should be noticed that the selection of the proper seed patch is important in the region-growing approach. Since the estimates of the parameters for the homogeneous region are updated while the patch expands, an improper choice of the seed patch could lead to an unreliable result in surface representation.

Proceeding in the same way as for selecting the queued sels, the selection of the seed for the next region is also queued according to the value of $\|\Psi_{patch}\|_2$ in search of the rest candidates.

The overall region-growing approach consists of the following steps:

1. Partition the range image into *sels*, and classify these sels as “ambiguous” or “ordinary”.
2. Estimate all the possible *patches* by merging a set of neighboring sels and applying the surface-fitting method described in Section 2. From these patches, select the seed patch that has the smallest value of *measure of uncertainty*.
3. Starting from the seed patch, the region is updated by merging its neighboring sels that pass the homogeneity test. The smaller the *measure of uncertainty* in merging the sel, the higher is the priority in the queue for merging. The region parameters are updated after each merge.
4. If all the neighboring sels of the current region fail to pass the homogeneity test, then the growing process stops and the current region is assigned a label.
5. For the remaining sels, repeat steps 2–4 to generate new-labeled regions. The whole process ends if no more patches are found.

At the end of the second module, we obtain a set of labeled regions, i.e., the *dominant regions* consisting of a set of sels. These dominant regions represent different clusters in parameter space for surface representations, but not an exact partitioning of the whole image in spatial domain. Points near the boundaries of these dominant regions should be treated in a refined process, i.e., these sels should be split at point level and further classified. This is implemented in the third module, as described below.

3.3. Point-based refinement

There are two kinds of sels that should be considered to pass through the refinement process: merged and non-merged. The merged sels are those at the boundary between two or more neighboring dominant regions. In this

situation, points in these boundary sels are reclassified as either their current segment or other neighboring segments. The non-merged sels adjacent to a dominant region are split down to points and these points are further classified as surface points of this adjacent segment or non-surface points. In both situations, the criterion for classification is based on the spatial “closeness” of a point to the specified surface. Simply, we can use the geometric distance between a point and a surface as the measure of such a spatial closeness.

Denoting by $d^2(\theta)$ the squared distance from point \mathbf{x} to the surface whose parameters are noted by θ , identification of a surface point is based on the comparison of $d^2(\theta)$ with a threshold. If $d^2(\theta) \geq T$, it is classified as a non-surface point. Otherwise, it is merged with the surface of θ . The value of $d^2(\theta)$ is approximately computed by $d^2(\theta) = h^2(\mathbf{x}, \theta) |\nabla h|^{-2}$, where $h(\cdot) = 0$ is the implicit quadric representation of the surface. Considering that the noise estimates might be different for different segments, we select the threshold $T = r_{point} c_{seg}$, where c_{seg} is the estimate of noise variance for the concerned segmentation and r_{point} is a constant.

If there is more than one surface for which the criterion is satisfied, then it becomes an optimal classification problem, in which case the point is classified as the surface in which the distance is the smallest.

It should be pointed out that in this process the outliers that are detected in the first module also participate in the classification. This is because some of the detected outliers are in fact surface points, but located near the boundaries or edges of the object. After reclassifying those points, the surface parameters of the refined segment are recomputed.

Finally, the outcomes of the third module are the labeled final segments and the unlabeled points.

4. Planarity test

In our approach, the planar primitives are distinguished with quadric primitives. Although a planar surface can also be represented by higher order polynomials, the representation could suffer from non-uniqueness of the solution. Intrinsically, fitting a planar data set to higher order polynomial is an ill-posed problem.

To avoid this problem, in the second module, where the region parameters are estimated, we apply a routine of planarity test to identify the planar surfaces. Then the planar surfaces are estimated using the planar representation instead of quadric representation and their region-growing proceeds with planar representations.

Suppose that $\{\mathbf{x}_i\}$ ($i = 1, \dots, n$) are points sampled from a planar surface and they are used to fit a quadric presentation of (1)

$$f(\cdot) = \mathbf{p}^T \mathbf{m} = 0, \quad (16)$$

where

$$\mathbf{m} = [x^2, y^2, z^2, xy, xz, yz, x, y, z, 1]^T \quad \text{and} \\ \mathbf{p} = [a_{11}, a_{22}, a_{33}, a_{12}, a_{13}, a_{23}, v_1, v_2, v_3, k]^T \quad \text{with } \|\mathbf{p}\|_2^2 = 1.$$

Using the fitting criterion

$$\mathbf{p} = \arg \min \left\{ \sum_{i=1}^n f_i^2 \right\}, \quad (17)$$

the solution of \mathbf{p} is given as the eigenvector of the matrix

$$\mathbf{M} = \sum_{i=1}^n \mathbf{m}_i \mathbf{m}_i^T, \quad (18)$$

associated with the smallest eigenvalue. In the noise-free ideal case, the smallest eigenvalue of \mathbf{M} is zero. However, since the solution of \mathbf{p} is non-unique, there are more than one eigenvectors with zero eigenvalue. Considering the normalization requirement for the algebraic coefficients, there are four eigenvectors with zero eigenvalues. Therefore, when ordering the ten eigenvalues as $\lambda_1 \geq \lambda_2 \geq \dots \geq \lambda_{10}$, ideally $\lambda_7 = \dots = \lambda_{10} = 0$.

Hence, we identify a planar patch in quadric representation just by checking the eigenvalue of λ_7 . Of course, in reality, the value of λ_7 is non-zero because of noise, but it can be expected that for very “flat” surfaces, this eigenvalue is small. Therefore, we can simply use a threshold T_{plane} to test the planar points. The criterion is as follows:

If

$$\left(\frac{\lambda_7}{n} \right) \leq T_{plane} \quad (n \text{ is the number of points}), \quad (19)$$

then the points belong to a planar surface, otherwise a quadric surface.

In the second module, the seed patch is searched from the candidate patches before the region-growing process. In this searching stage, each patch is subjected to the planarity test. Of all the planar patches that are found, a seed is selected and the growth is carried out in planar representation.

5. Experimental results

The algorithm presented in Sections 2, 3 and 4 has been applied to real range images² and synthetic range data. The experiments were carried out following the flowchart of Fig. 1. Four different scenes with trials for each were used to test the proposed approach. The scenes include a flat background and objects that are assumed being modeled with either quadric or planar surface primitives.²

² The range images were obtained with the ranging system of the Measurement & Instrumentation Laboratory, University of Twente.

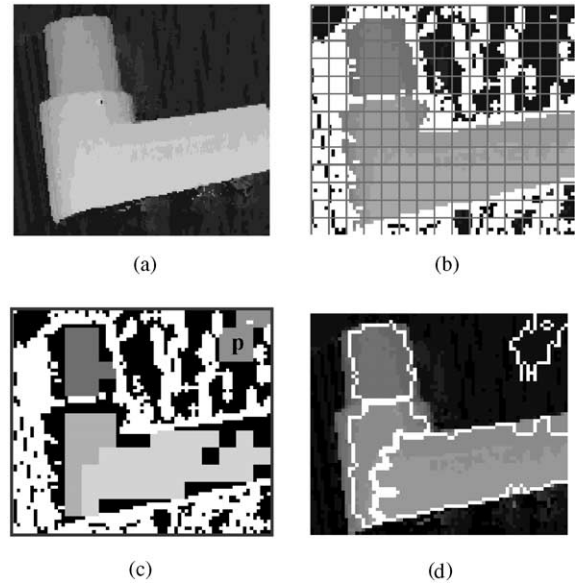


Fig. 3. Segmentation results with real range images. Picture (a) is the original range image (depth value is mapped to graylevel). (b) Shows the result of outlier detection (the bright pixels), where the initial grid of sels is also displayed. (c) Shows the result of merging sels. The labeled segments, i.e., the dominant regions, are shown with different graylevels (outliers are also displayed with higher brightness). (d) Shows the final segmentation result after the refinement step. Of the dominant regions in picture (c), the planar regions have been marked with letter “p”, others are regarded as quadric regions.

Figs. 3–6 show the segmentation results for the four scenes. For each of them, a set of images is arranged to display the results:

- Original input range image. The depth value is mapped to the grayscale.
- The result of outlier detection by the first module, in which the detected outliers are displayed highlighted (white points). The whole image has been initially segmented with a grid of sels.
- The result of region growing by the second module. Merging of homogeneous sels results in dominant regions (displayed in different graylevels).
- Final result of point-based refinement by the third module. Primitives are extracted as the regions bounded by the white curves.

In order to reduce the computational burden and the degree of correlation between neighboring pixels, each range image was resampled at a lower resolution. For the inputs of Figs. 3, 4 and 6 the resampling resolution was 2 pixels/point, but for Fig. 5 it is 3 pixels/point. The used range data in our computation were the set of resampled points.

In the first module, the size of the window used to detect the outlier is 5×5 (point²) and $r_{win} = 25$ in the threshold of

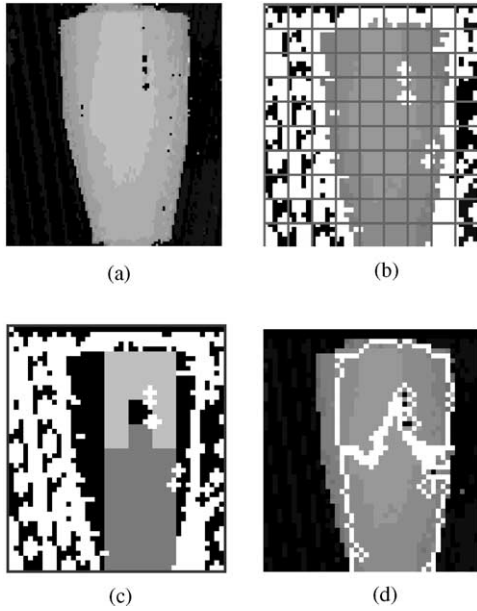


Fig. 4. Segmentation result of real range image.

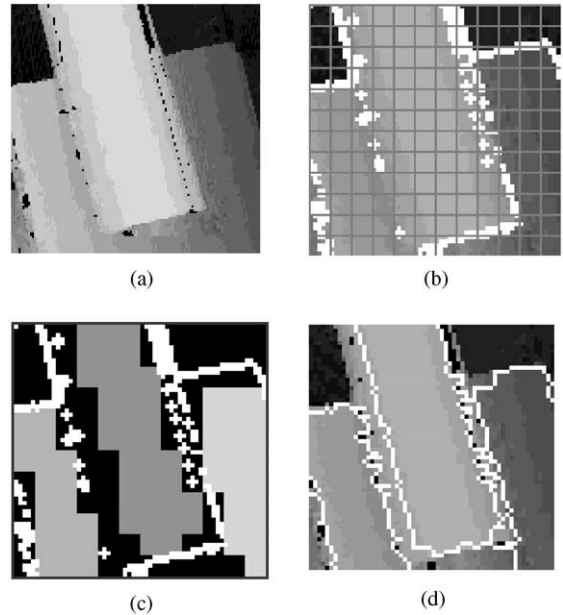


Fig. 6. Segmentation results of real range image.

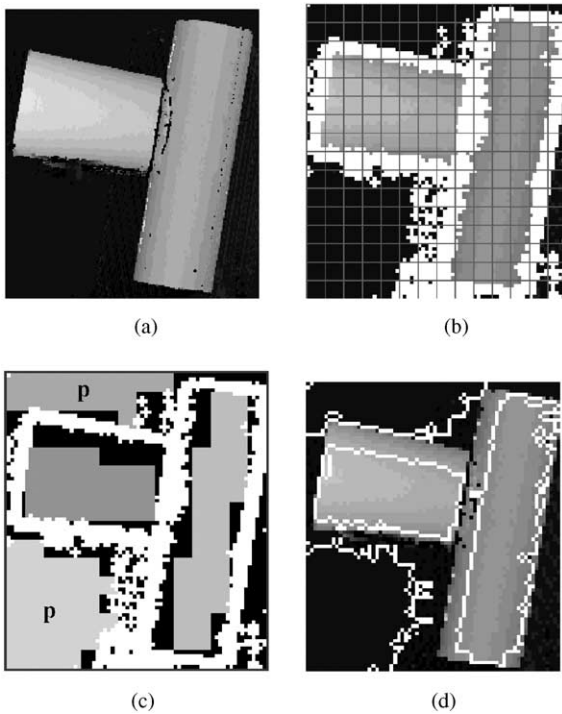


Fig. 5. Segmentation results of real range image.

Eq. (14). In addition, if the depth value of the centered point differs from one of its (4-connective) neighboring points over a threshold $T_{depth} = 1$ (mm), that centered point is also

marked as an outlier. In the beginning of the second module, the whole image is manually partitioned into grid-sized *sels*. The size of each sel in the experiments is 5×5 (point²). If a sel contains a number of outliers exceeding a pre-defined fraction, i.e., 20% of the total points in a sel, then this sel is marked as “ambiguous” and will not participate in the merging process. All others are considered to be “ordinary” sels. Selection of the seed *patch* and the order of merging the ordinary sels were ruled by the principle as stated in Section 3.2. Except for the homogeneity test, another criterion to control the merging process is that if there are enough points in the sel whose distances to the current surface exceed a certain threshold (these points are regarded as non-fitted points), the current merging is rejected. The threshold of distance is $d^2 \geq r_d d_{med}^2$, where d_{med}^2 is the median of the squared distances within the sel, while the constant used in the experiment is $r_d = 25$. The threshold of the number of non-fitted points was $T_n = 20\%$ of the total number of the sel.

An important parameter in the merging process is the threshold T_d for the “optimal distance”. Usually, a large value of T_d may cause under-segmentation, whereas a small value of T_d could cause over-segmentation. In practice, the value of T_d should be selected empirically. In our experiments, we set the value of T_d by referring to the histogram of the optimal distances between all the candidate seed patches and their neighboring sels. We experimentally set T_d around the last peak of the histogram, which is thought to be the bound of the “most possible” distances between two homogeneous estimates. The selected values of T_d and the histograms for the instances of Figs. 3–6 are depicted

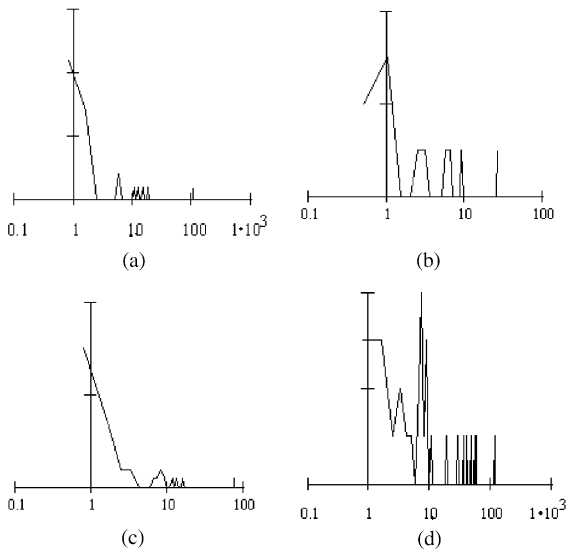


Fig. 7. The histogram of d_s^2 in the process of searching the seed patch. The x co-ordinate is on a log-scale. The values of T_d as used in the experiments are also given. (a) Result with respect to Fig. 3. The used threshold $T_d = 30$. (b) Result with respect to Fig. 4. The used threshold $T_d = 15$. (c) Result with respect to Fig. 5. The used threshold $T_d = 90$. (d) Result with respect to Fig. 6. The used threshold $T_d = 80$.

in Fig. 7. According to our experiments, small changes in the value of T_d (for example, variation within $\pm 20\%$) did not significantly change the segmentation results. This also illustrates that the optimal distance yields a reliable measure for *class separability*.

In the experiments, the threshold for the planarity test in Eq. (19) was set to $T_{plane} = 0.0005$. At the end of region growing, a group of the merged sels is labeled as a *dominant region*, as shown in (c) of Fig. 3. In the third module, these dominant regions are refined by reclassifying non-merged points. All the neighboring sels of these dominant regions, whether ambiguous or ordinary, are split at point level. The threshold distance in order to identify a non-surface point was selected as $T_{pointdist} = 0.8$ mm. Points whose distance exceeds this threshold and those in isolated sels were all marked as “unlabeled”. In these segmentation results, the planar segments were marked with the character “p”, while others were in quadric representation.

It should be pointed out that in experiments, some regions that were considered as planar (e.g. the supporting plate of the cylinder in Fig. 6) were tested as quadric and have grown in the quadric representation. This is due to noise perturbation in the input range images, leading to errors in the shape description of the planar patch. Of course, if the threshold T_{plane} in the planarity test increases, then more regions could be recognized as being planar. In order to avoid an over-segmented result, we prefer reducing the risk of treat-

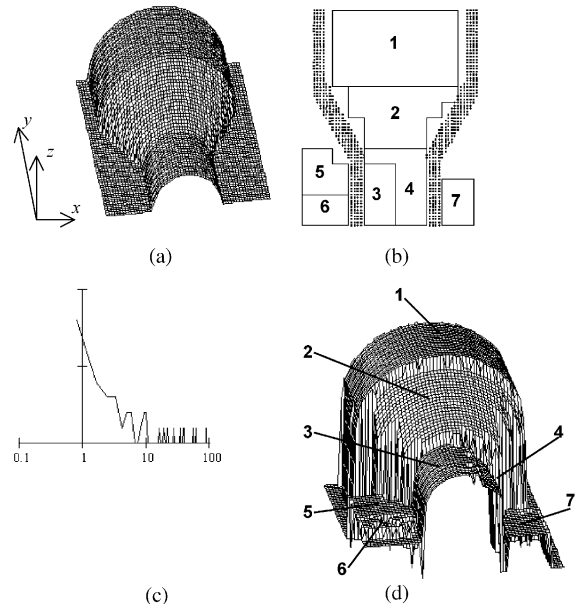


Fig. 8. Segmentation result with synthetic data. (a) The scene consisting of synthetic data. The radius of the larger cylinder is 20. The sampling interval is 0.8. Gaussian noise of standard deviation $\sigma = 0.02$ has been added to the three co-ordinates for each point (in the picture, noises are only added to z-co-ordinates for the purpose of plotting). (b) The perspective view of the dominant regions by merging sels. The size of the sel is 4×4 . The seven regions are labeled with Figs. 1–7. (c) The result of the histogram of d_s^2 . The used parameter $T_d = 100$. (d) The final result of refinement. The figured regions correspond to the labels in (b). In order to view different segments, labeled regions have been detached at the z direction.

ing a curved patch in planar description. In fact, the reason to separate planar and quadric representations is to avoid the possible ill-posed problem when fitting low-dimensional surface data to a higher dimensional representation. As long as the ill-posed problem is tolerated, a low threshold value for T_{plane} is recommended.

From the experiments, it can be noticed that the boundary points of a curved surface were usually difficult to be merged. This might be due to inaccurate range data acquisition at the boundaries. Such results seem “imperfect” according to our perceptual experiences. However, as argued at the beginning of this paper, in the sense of primitive extraction, what we are concerned with and expect from the segmentation is the reliability of surface representation. A “visually pleasing” judgement for range image segments should be discarded.

The segmentation algorithm was also applied to synthetic data. In Fig. 8(a), the 3D scattered data points generated from a synthetic object surface and a planar background are depicted. Gaussian noise has been added to the three co-ordinates of each point. The standard deviation of

Table 1
Estimated parameters of the segmented surfaces of the object in Fig. 8

	Estimate of surface parameters	Actual values
1	8.2×10^{-5} , 0, 8.3×10^{-5} , 0, 0, 0, -0.016464, -0.000037, -0.008264	8.3×10^{-5} , 0, 8.3×10^{-5} , 0, 0, 0, -0.016529, 0, -0.008264
2	1.06×10^{-4} , -3.4×10^{-5} , 1.02×10^{-4} , 0, 1×10^{-6} , 4×10^{-6} , -0.021221, 0.006540, -0.010630	1.06×10^{-4} , -3.3×10^{-5} , 1.06×10^{-4} , 0, 0, 0, -0.021246, 0.006557, -0.010623
3	8.1×10^{-5} , 0, 8.2×10^{-5} , 0, -2×10^{-6} , -1×10^{-6} , -0.016155, -0.000032, -0.007954	8.1×10^{-5} , 0, 8.1×10^{-5} , 0, 0, 0, -0.01613, 0, -0.008064
4	3.2×10^{-5} , 0, 5.5×10^{-5} , -2×10^{-6} , 8.9×10^{-5} , -6×10^{-6} , -0.011376, 0.000846, -0.015185	

Their actual values are also given.

the noise is $\sigma = 0.02$. The sampling interval at x and y directions is 0.8.

The same segmentation approach was applied as for the images in Figs. 3–6. Also, the parameters have been selected to be the same, except for the threshold of the optimal distance in the merging criterion, which is set to $T_d = 100$, and the size of the sel, now being 4×4 . The segmentation result of the dominant regions is illustrated in Fig. 8(b) with a perspective view at the z direction. The histogram of d_s^2 is depicted in Fig. 8(c). Finally, the seven segmented regions are shown in Fig. 8(d) after applying the process of point-based refinement (in exploded view along the z direction, for the purpose of visualization).

A notable result of the segmentation is that the bottom cylinder portion in Fig. 8(b) was over-segmented into two regions, i.e., labels “3” and “4”. This was caused by noise perturbation in the data points. However, according to the final estimate of the surface parameters for each segment, it can be found that one of the two segments of this over-segmented cylinder surface, i.e., label “3”, has well recovered the true parameters of this cylinder representation. But the other gives an unexpected result. This result significantly revealed the advantage of the proposed approach for a primitive extraction in range image segmentation. The estimated surface parameters of the object surface regions and the actual surface parameters are listed in Table 1.

6. Conclusions

This paper presented a new estimation-based approach for range image segmentation. The core of the approach is the optimization of the surface description. Since the uncertainty in an estimate of region parameters is explicitly represented with a covariance matrix, the definition of homogeneity and the clustering criterion can be established within an optimal framework. To do that, we applied a probabilistic model

with normal pdf to characterize the statistical properties of a region’s estimate.

Our algorithm interprets the range image segmentation as a phase of primitive extraction of the scene. Thereby, the reliability of primitive representation and extraction is emphasized. Currently, the first- and second-order polynomials are used to model the surface primitives. We defined the “measure of uncertainty” as a test of the reliability of a single estimate, which turns out to control the extraction of the surface primitive. Therefore, the problem of order of merging in region-growing methods is solved by the criterion of *reliability* of primitive representation. The new spirit in the proposed algorithm is—the range images segmentation is not thought of as “how the scene is partitioned”, but is thought of as “how the scene is reliably described”. Experimental results have proved the effectiveness of the algorithm and the applicability of such a spirit.

A susceptible question in using this method is the determination of the parameter T_d , the threshold of the optimal distance in the homogeneity test. It is not realistic to fix this parameter for all kinds of range images. A solution to determine this parameter is to refer the histogram of the optimal distance between the candidate seed patches and their neighboring sels, which has been proved effective in our experiments. More systematically, we can consider the number of final clusters in a given scene as a priori information. This relates to the research work on the specification of the number of clusters called *cluster validation* [21,22], in which the number of clusters is determined by the maximum entropy principle.

7. Summary

We proposed a new estimation-based approach for range image segmentation with a region-growing scheme. The objects were modeled with quadric or planar surface representations and the segmentation is interpreted as a process

of primitive extraction. The proposed algorithm focused on the “reliability” of the extracted surface primitive representation.

Elementary in this segmentation algorithm is the optimal description of the surface primitives. We established a probabilistic model with normal pdf to describe the estimate of surface parameters, combined with the covariance computation in surface fitting. Consequently, the optimization in estimation-based segmentation is realized with two outputs: (1) the homogeneity of two region estimates is tested with a criterion of “optimal distance”; (2) the uncertainty in a region estimate is explicitly described, as the novelty in our approach, by defining a metric of “measure of uncertainty” in terms of the *norm* of the covariance matrix. The second output induces a solution for the problem of “order of merging” in the region-growing method—the region always grows towards the most reliable description of the final extracted primitive, i.e., the “measure of uncertainty” being minimum.

The segmentation approach consists of three modules:

Outlier detection. To keep the smoothness constraint in surface fitting, extraordinary error points and the edge/boundary points are preliminarily extracted by local operation. A square mask is used to test the central point by computing the goodness of planar fitting with the mask. These outliers do not participate in surface fitting in the second module.

Estimation-based region growing. Initially, the range image is manually partitioned into a set of regular grid pattern. Then the region-growing process starts with these “surface elements” (*sels*). A subregion (*patch*) is selected as the seed of growing. Region parameters are estimated by incorporating the covariance computation, and the current region grows by merging the neighboring *sels*. The order of merging is determined by the metric of “measure of uncertainty”. A threshold of the “optimal distance” is selected to test the homogeneity of the regions before and after merging a *sel*. We select the threshold by checking the histogram of the “optimal distance” between the candidate seed patches and their neighboring *sels*.

In this stage, a planarity test routine is applied to distinguish quadric surfaces to planar surfaces. A patch identified as planar then grows in planar representation.

At the end of this stage, the range image is partitioned into a set of labeled regions consisting of the merged *sels* (*dominate region*).

Point-based refinement. All the points in the neighborhood of the dominant regions (including the outliers) are reclassified to be surface points or non-surface points by checking the geometric distance between a point and the dominant regions. Finally, the whole range image is segmented into labeled segments and unlabeled points.

The proposed approach has been applied to the segmentation of real range images and synthetic data. The experimental results demonstrated the effectiveness of the approach proposed in this paper.

References

- [1] A. Hoover, et al., An experimental comparison of range image segmentation algorithms, *IEEE Trans. Pattern Anal. Mach. Intell.* 18 (7) (1996) 673–689.
- [2] P.J. Besl, R.C. Jain, Segmentation through variable-order surface fitting, *IEEE Trans. Pattern Anal. Mach. Intell.* 10 (2) (1988) 167–192.
- [3] J.H. Han, R.A. Volz, T.M. Mudge, Range image segmentation and surface parameter extraction for 3-D object recognition of industrial parts, *Proceedings of the IEEE International Conference on Robotics and Automation*, Raleigh, NC, USA, Vol. 1, 1987, pp. 380–386.
- [4] R. Hoffman, A.K. Jain, Segmentation and classification of range images, *IEEE Trans. Pattern Anal. Mach. Intell.* 9 (5) (1987) 608–620.
- [5] M. Oshima, Y. Shirai, Object recognition using three-dimensional information, *IEEE Trans. Pattern Anal. Mach. Intell.* 5 (4) (1983) 353–361.
- [6] R.W. Taylor, M. Savini, A.P. Reeves, Fast segmentation of range imagery into planar regions, *CVGIP* 45 (1989) 42–60.
- [7] G.Y. Wang, Recognition of man-made objects from range data: optimization of surface based (quadric) representation, Ph.D. Thesis, University of Twente, The Netherlands, 2000.
- [8] A.P. Davignon, Detecting orientation discontinuities in range images by use of directional derivatives, *Proceedings of the IAPR 11th International Conference on Pattern Recognition*, Hague, The Netherlands, Vol. 3, 1992, pp. 455–458.
- [9] T.J. Fan, G. Medioni, R. Nevatia, Surface segmentation and description from curvature features, *Proceedings of the Image Understanding Workshop, Advanced Research Projects Agency*, Los Angeles, CA, 1987, pp. 351–359.
- [10] W.E.L. Grimson, T. Pavlidis, Discontinuity detection for visual surface reconstruction, *CVGIP* 30 (1985) 316–330.
- [11] S. Kaveti, E. Khwang, H. Wang, Second-order implicit polynomials for segmentation of range images, *Pattern Recognition* 29 (6) (1996) 937–949.
- [12] G. Taubin, Estimation of planar curves, surfaces, and nonplanar space curves defined by implicit equations with applications to edge and range image segmentation, *IEEE Trans. Pattern Anal. Mach. Intell.* 13 (11) (1991) 1115–1138.
- [13] S.M. LaValle, S.A. Hutchinson, A Bayesian segmentation methodology for parametric image models, *IEEE Trans. Pattern Anal. Mach. Intell.* 17 (2) (1995) 211–217.
- [14] D. Keren, D. Cooper, J. Subrahmonia, Describing complicated objects by implicit polynomials, *IEEE Trans. Pattern Anal. Mach. Intell.* 16 (1) (1994) 1–13.
- [15] B. Sabata, F. Arman, J.K. Aggarwal, Segmentation of 3D range images using pyramidal data structures, *CVGIP: Image Understanding* 57 (3) (1993) 373–387.
- [16] J. Subrahmonias, D. Cooper, D. Keren, Practical reliable Bayesian recognition of 2D and 3D objects using implicit polynomials and algebraic invariants, *IEEE Trans. Pattern Anal. Mach. Intell.* 18 (5) (1996) 505–519.
- [17] O.D. Faugeras, M. Herbert, E. Pauchon, Segmentation of range data into planar and quadratic patches, *Proceedings of the Third Computer Vision and Pattern Recognition Conference*, Arlington, VA, USA, 1983, pp. 8–13.

- [18] K. Kanatani, Statistical bias of conic fitting and renormalization, *IEEE Trans. Pattern Anal. Mach. Intell.* 16 (3) (1994) 320–326.
- [19] Z. Zhang, Parameter estimation techniques: a tutorial with application to conic fitting, *Image Vision Comput.* 15 (1997) 59–76.
- [20] P. Whaite, F.P. Ferrie, From uncertainty to visual exploration, *IEEE Trans. Pattern Anal. Mach. Intell.* 13 (10) (1991) 1038–1049.
- [21] A.K. Jain, Cluster analysis, in: T.Y. Young, K.S. Fu (Eds.), *Handbook of Pattern Recognition and Image Processing*, Academic Press, New York, 1986.
- [22] J. Zhang, J.W. Modestino, A model-fitting approach to cluster validation with application to stochastic model-based image segmentation, *IEEE Trans. Pattern Anal. Mach. Intell.* 12 (10) (1990) 1009–1017.

About the Author—GUOYU WANG was born in Qingdao, China, on 27 January 1962. He received the B.Sc. and M.Sc. degrees in Physics in 1984 and 1987, respectively, from the Department of Physics, Ocean University of Qingdao, China. Subsequently, he worked as a staff member at the Department of Physics and then at the Department of Electrical Engineering, Ocean University of Qingdao. During 1993–1994 and 1990–2000, he did research as a visiting scholar in the Department of Electrical Engineering, University of Twente, The Netherlands, and obtained the Ph.D. degree from the University of Twente in 2000. He is currently an associate professor in the Department of Electrical Engineering, Ocean University of Qingdao. His research interests include image processing, pattern recognition and machine vision.

About the Author—ZWEITZE HOUKES was born in Utrecht, The Netherlands, on 30 October 1939. He received the M.Sc. and Ph.D. degrees from the Delft University of Technology and the University of Twente, The Netherlands, in 1963 and 2000, respectively. During 1961–1968, he served as a researcher in Philips Telecommunication Industries and then in Dutch Railway. Since 1969 he has been working as a staff member in the Department of Electrical Engineering, University of Twente, The Netherlands, and currently he is an associate professor. He is a member of IAPR and IEEE and the scientific committee of the Advanced School for Computing & Imaging, The Netherlands. His current research fields include computer vision, pattern recognition, signal processing and image-based measurement.

About the Author—GUANGRONG JI was born in Shandong province, China, on 10 October 1953. He received the B.Sc. degree in 1976 from the Department of Physics, Ocean University of Qingdao, China. Subsequently, he has been working in the Department of Physics and in the Department of Electrical Engineering, Ocean University of Qingdao. He is currently a professor and the Dean of the Department of Electrical Engineering, Ocean University of Qingdao, and a senior member of China Electronics Association. His research interests include image processing, pattern recognition and machine vision.

About the Author—BING ZHENG was born Qingdao, China on 7 November 1968. He received the B.Sc. and M.Sc. degree in 1987 and 1995, respectively, from the Department of Electrical Engineering, Ocean University of Qingdao. Since 1988, he has been a lecturer in the same department. His current research interests include robotics and image processing.

About the Author—XIN LI was born in Qingdao, China on 27 January 1959. He received the B.Sc. degree in 1981 from the Department of Electrical Engineering, Zhejiang University, China. Subsequently, he worked as a staff member in the Department of Electrical Engineering, Ocean University of Qingdao. He is currently an associate professor in the Department of Electrical Engineering, Ocean University of Qingdao. His research interests include signal processing, robotics and machine vision.